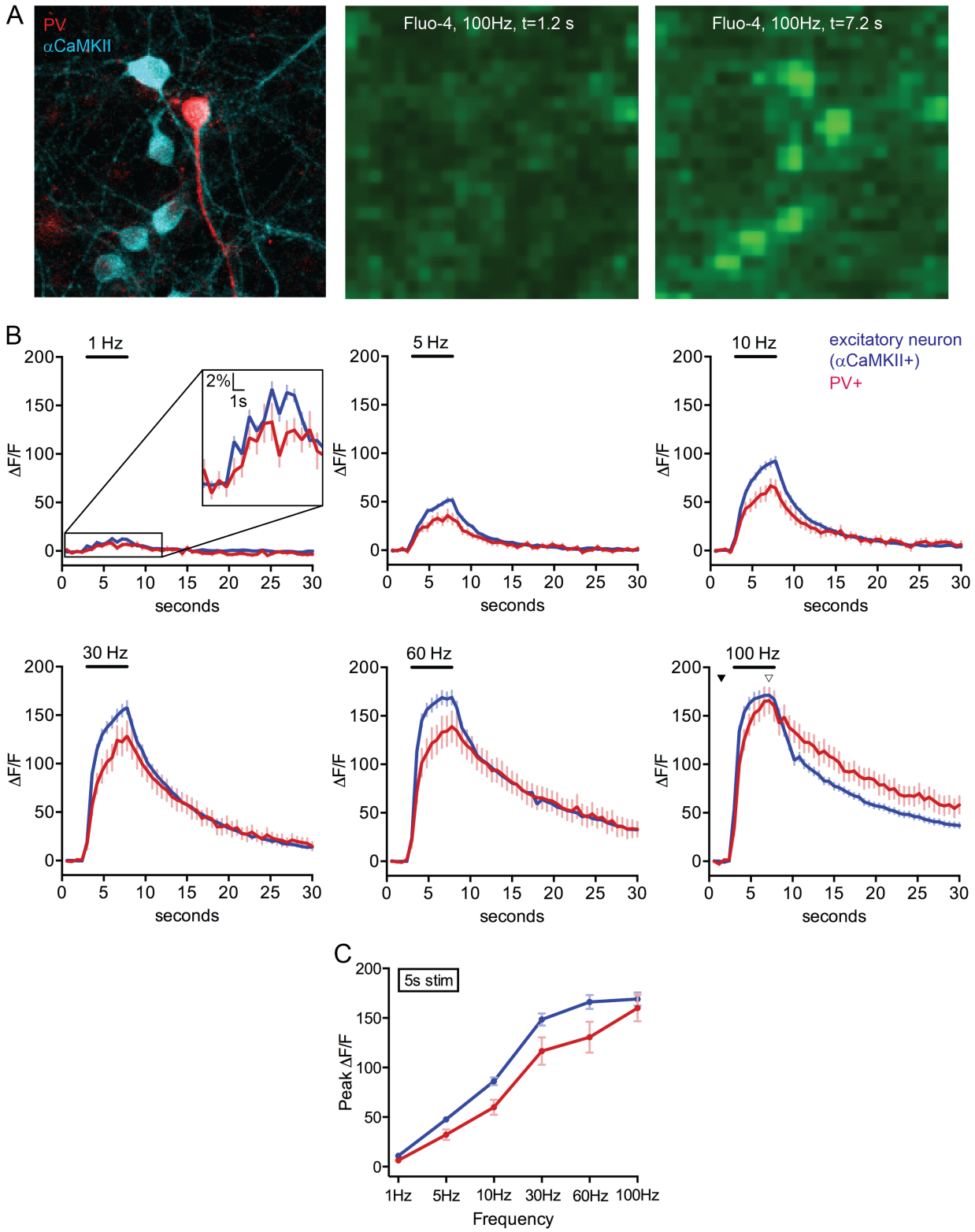

Figure S1, Related to Figure 1. Ca^{2+} Imaging in Cultured PV+ Interneurons and Excitatory Neurons

(A) Left, co-staining of PV (red) and excitatory neuron marker αCaMKII (cyan) in rat cortical cultures, subjected to 100 Hz stimulation (applied from 2.5 s to 7.5 s). Middle and right, Fluo-4 signal (green) from the same cells shown

at left, at the time point indicated. Black and white triangles in the bottom right panel of (B) indicate respectively the time points at which middle and right panels were taken.

(B) Cultured neurons were given 5 s trains of field stimulation at 1 Hz, 5 Hz, 10 Hz, 30 Hz, 60 Hz, or 100 Hz. The inset in the top left panel shows how excitatory neurons, but not PV+ interneurons, were more obviously responsive to single action potentials. Recordings were obtained from PV+ neurons (n = 15) or αCaMKII+ (excitatory) neurons (n = 95), from 9 separate cover slips, all in the presence of NBQX and APV. Data are represented as mean±SEM.

(C) Plot of peak ΔF/F (%) vs. frequency of stimulation in PV+ cells (red) and putative excitatory neurons (blue), constructed from data shown in B. The frequency-response relation for PV+ interneurons was right-shifted along the frequency axis by ~2-fold relative to excitatory neurons. Data are represented as mean±SEM.

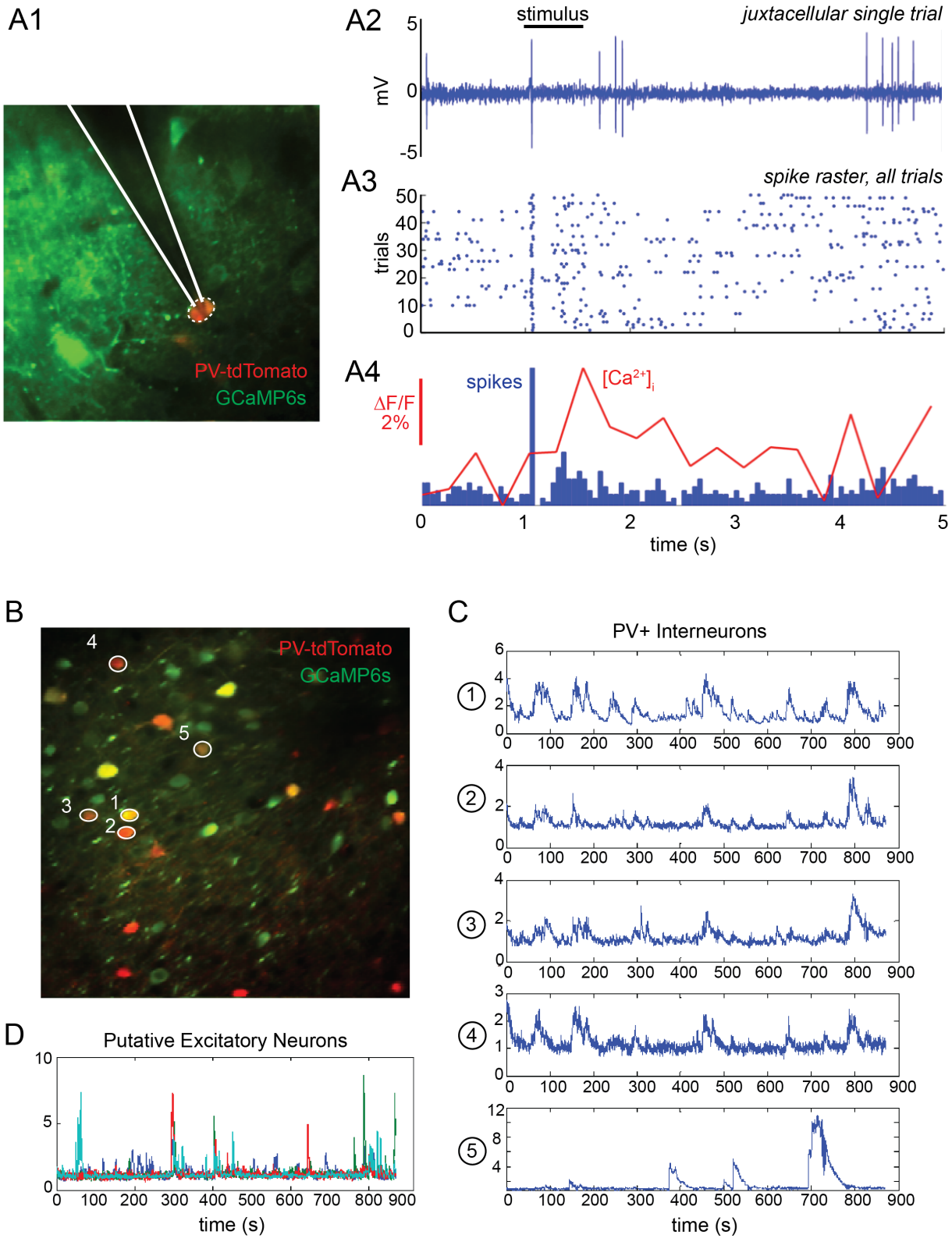

Figure S2, Related to Figure 1. Ca^{2+} Imaging of PV+ Interneurons *in vivo*

(A1) Two-photon image of auditory cortex with a patch electrode (outline in solid white) targeted to a PV+ interneuron (outline in dashed white). GCaMP6s (green) was expressed pan-neuronally in mice that expressed tdTomato (red) only in PV+ neurons. Neurons expressing both GCaMP6s and tdTomato were targeted to test whether GCaMP6s could reliably detect single action potentials arising from a sound-evoked stimulus. (A2) An unfiltered raw trace of a juxtacellular recording showing a stimulus-evoked spike (white noise, 70 dB) along with spontaneous activity. (A3) spike raster plot (50 trials) showing the reliable spiking response to the stimulus together with ongoing activity typical of a PV+ neuron. (A4) Peristimulus time histogram of the juxtacellularly-recorded spikes (blue), overlaid with the average calcium signal (red).

(B) Exemplar image of mouse auditory cortex with putative excitatory neurons (green) and PV+ positive cells (red, PV-tdTomato; green, GCaMP6s), as in Figure 1D. White circles represent multiple regions of interest used for image analysis in (C).

(C) Individual spontaneous GCaMP6s ($\Delta F/F$) responses from the PV+ cells identified in (B). Note that Ca^{2+} transients lasting tens of seconds are separated by gaps in activity.

(D) Individual spontaneous gCaMP6s ($\Delta F/F$) responses from putative excitatory neurons in the same field of view as the PV+ cells shown in (C).

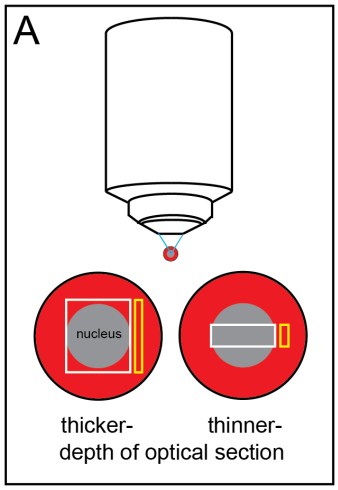

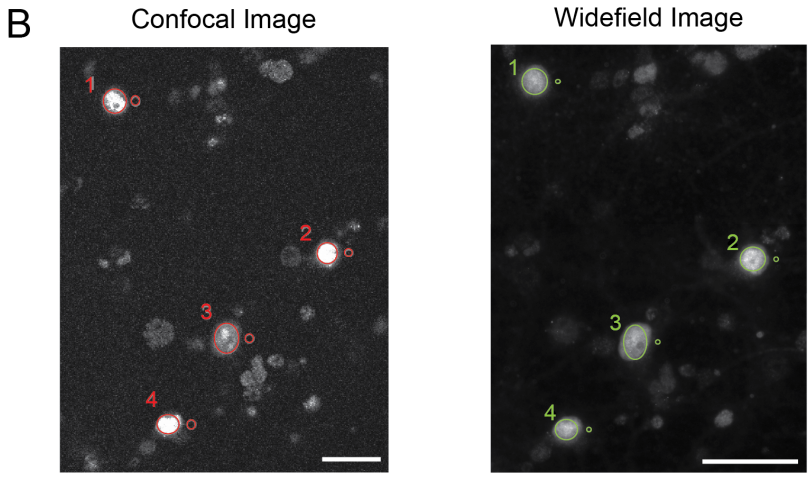

cell number	1	2	3	4
nuclear ROI intensity	49499	56656	31947	57843
juxtanuclear ROI intensity	5719	5911	5426	6423
ratio	8.66	9.58	5.89	9.01

1	2	3	4
3902	5910	4177	4975
557	686	707	699
7.01	8.62	5.91	7.11

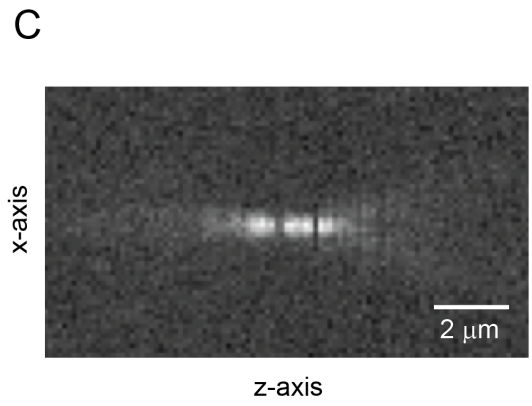

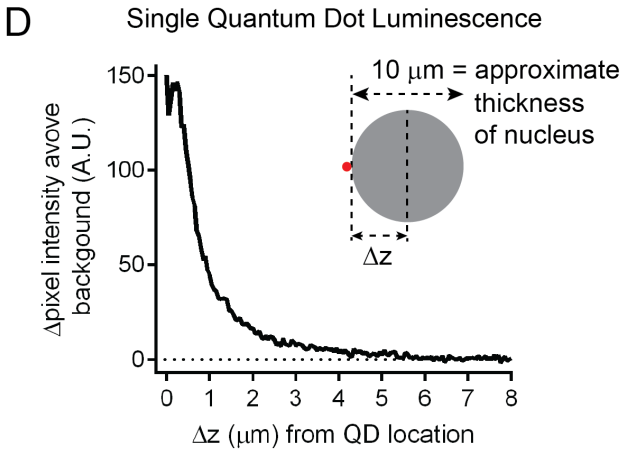

Figure S3, Related to Figure 2. The z-axis Resolution of Widefield Microscope Is Suitable for Spatial Analysis of Immunostaining Intensity in Cultured Neurons

(A) When the objective is focused on a given object such as the nucleus, a thicker optical section would result in contamination of the nuclear intensity (shown in gray in cartoon) with fluorescence from the cytoplasm above and below the nucleus (shown in red in cartoon). Confocal microscopes are often used to obtain a thin optical section.

For practical considerations, most images in this study were taken on a Zeiss Axio Imager M2 widefield microscope using a "PlanApochromat" 63x/1.40 Oil DIC M27 objective. The immersion oil had a refractive index n_e= 1,518 at 23^o C. Based on these parameters, excitation light at 470 nm would yield an optical section thickness of 313 nm for the full width at tenth maximum of the peak of PSF and a standard deviation (σ) of 72.9 nm for the Gaussian approximation of the PSF in the axial direction. 647 nm excitation light would give corresponding values of 433 nm and 101 nm. Based on these calculations the optical section thickness would be ~0.4 μm, much thinner than the

typical z-width of the nucleus, ~10-15 μm, so that fluorescence from cytoplasm above or below the nucleus would have negligible impact on the measured nuclear intensity.

(B) To assess experimentally the impact of optical section thickness, we compared confocal and widefield images of the same four cells, stimulated for 1 min with 40K and stained for pCREB S133. The respective images were acquired with a 63x objective on either a confocal (Zeiss LSM 510 meta Imager.M1) or a widefield (Zeiss Imager M.2) microscope and analyzed using ImageJ software. The pixel intensity of a nuclear ROI (represented by white box in (A)) and a juxtanuclear ROI (represented by yellow box in (A)) was calculated for each cell, and the nuclear/juxtanuclear ratio was calculated. Significant contamination from the cytoplasm would reduce the ratio (as the juxtanuclear region displays far less pCREB staining than the nucleus). This ratio was slightly lower in the cellular images taken with the widefield microscope, but the difference was small, suggesting that the widefield microscope is a suitable tool for our purposes. Scale bar, 40 μm.

(C) Empirical determination of z-axis resolution of our epifluorescence microscope, using a single 15 nm-diameter quantum dot (QD). Variation of image intensity was recorded as optical plane of section was advanced from beneath, up to, and through z-axis position of the exemplar QD. Note that intensity falls off sharply at distances of <2 μm from QD position.

(D) Average analysis (n = 25 QDs) of z-axis dependence of point spread function based on data in (C). $|\Delta z|$-dependence of intensity, assessed by averaging intensities measured both proximal and distal to QD location. Intensity falls off to 37% at $|\Delta z| = 0.83$ μm. Inset, cartoon showing a fluorescent object just outside a neuronal nucleus of typical size (10 μm). Within an optical plane of section at the midsection of the nucleus, contamination from a point source of perinuclear fluorescence would be ~ 3% of its maximal value.

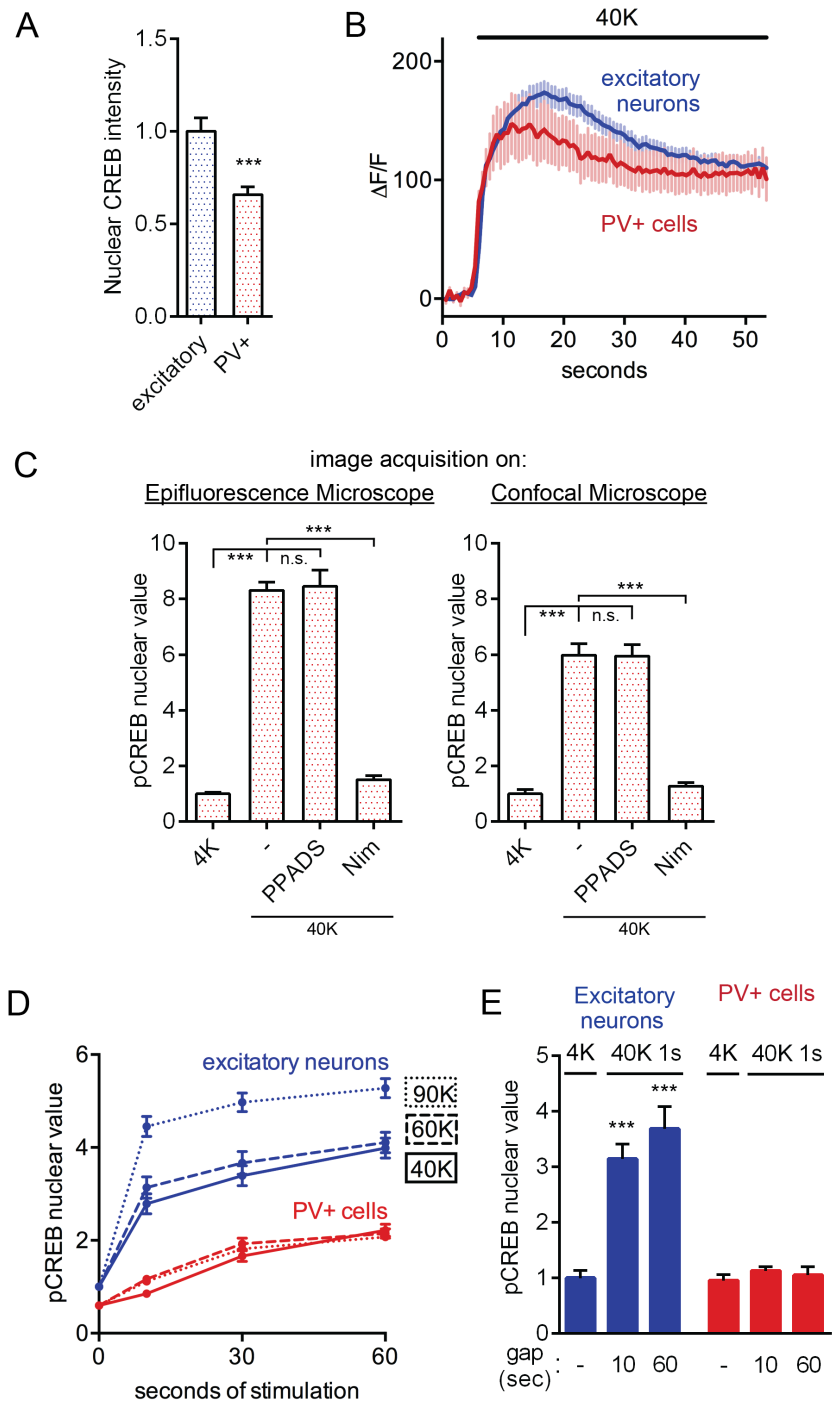

Figure S4, Related to Figure 2. Depolarization-triggered CREB Phosphorylation Is Different in PV+ cells and Excitatory Neurons

(A) PV+ cells have significantly less immunostaining for total CREB than excitatory neurons. Data are represented as mean+SEM. ANOVA followed by *t*-test. ***, $p \leq 0.001$.

(B) Depolarization with 40K triggers Ca^{2+} increases in PV+ cells and in excitatory neurons. Black bar represents duration of 40K stimulation. Data are represented as mean±SEM.

(C) 40K for 1 min triggers CREB phosphorylation in PV+ cells that is unaffected by P2 receptor antagonist PPADS

(30 μM) ($p = 0.83$, t-test), but prevented by nimodipine. The same result was seen when cells were analyzed with either epifluorescence (left panel) or confocal (right panel) microscopy. This supports the importance of Ca_V-derived Ca^{2+} and rules out the contribution of an indirect pathway triggered by glial ATP (Newman, 2003). All values were normalized to the mean basal condition value. Data are represented as mean+SEM. ANOVA followed by *t*-test. ***, $p \leq 0.001$.

(D) Time course of CREB phosphorylation in response to 40K (solid line), 60K (dashed line), and 90K stimulation (dotted line) in PV+ cells (red) and excitatory neurons (blue). All values were normalized to the mean baseline value for excitatory neurons. Data are represented as mean±SEM. TTX, APV, and NBQX were present.

(E) CREB phosphorylation in excitatory neurons (blue) and PV+ cells (red) in response to 40K depolarization for 1 s, followed by a gap of variable time prior to fixation. "-" represents basal condition prior to stimulation. Numbers at bottom refer to length of time gap (s) between end of stimulation and fixation. All values were normalized to the mean basal condition value for each cell type. Data are represented as mean+SEM. ANOVA followed by *t*-test. ***, $p \leq 0.001$.

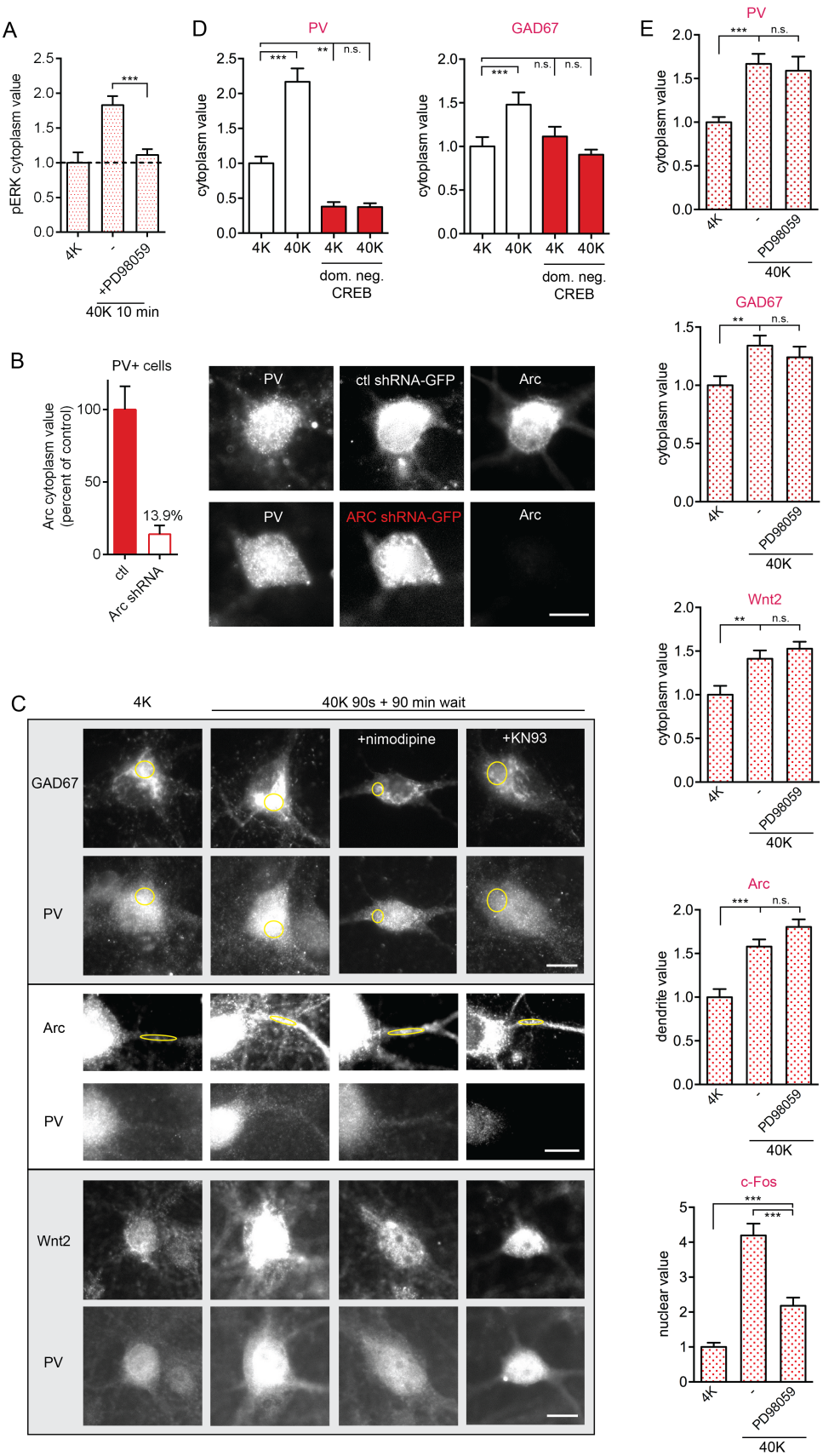
A
pERK cytoplasm value
4K
-
+PD98059
40K 10 min
D
PV
GAD67
cytoplasm value
dom. neg. CREB
E
PV
GAD67
Wnt2
Arc
c-Fos
dendrite value
nuclear value
PD98059
40K
B
PV+ cells
Arc cytoplasm value (percent of control)
13.9%
ctl
Arc shRNA
ctl shRNA-GFP
ARC shRNA-GFP
Arc
C
4K
40K 90s + 90 min wait
+nimodipine
+KN93
GAD67
PV
Arc
Wnt2

Figure S5, Related to Figure 3. Depolarization-dependent, MAPK-independent Signaling Is Responsible for Upregulation of Multiple CREB Target Genes

(A) The MEK inhibitor PD98059 prevented the increase in pERK formation, seen after 10 min of 40K depolarization. All values were normalized to the mean basal condition value. Data are represented as mean+SEM. ANOVA followed by *t*-test. ***, $p \leq 0.001$.

(B) Left, Arc shRNA reduces cytoplasmic Arc levels by ~86% in PV+ cells. Right, top row of images shows a representative control cell, which was transfected with a control shRNA that expressed GFP on the same plasmid, and co-stained for Arc and PV. The bottom row shows a representative knockdown cell, which was transfected with an Arc shRNA construct that expressed GFP on the same plasmid, and co-stained for Arc and PV. These data support the specificity of the Arc antibody and the expression of Arc in cortical PV+ cells. Scale bar, 10 μm.

(C) Representative images of co-staining for PV/GAD67, PV/Arc, or PV/Wnt2. Cells were either depolarized with 40K for 90 s or mock-stimulated in 4K, and then incubated under basal conditions for 90 min before fixation. Note that treatment with nimodipine or KN93 prevented the stimulation-induced increases in immunostaining for all genes. Yellow circles in first three rows are representative cytoplasmic (top two rows) or dendritic (third row) regions-of-interest chosen for determination of average pixel intensity. Scale bar, 10 μm.

(D) Left, expression of a dominant-negative CREB construct (dom. neg. CREB) lowered basal levels of PV expression and prevented increases in PV that were triggered by 40K for 90 s, followed by a 90 min rest period. Right, the dom. neg. CREB lowered basal levels of GAD67 expression and prevented increases in GAD67 that were triggered by 40K for 90 s, followed by a 90 min rest period. All values were normalized to the mean basal condition value. Data are represented as mean+SEM. ANOVA followed by *t*-test. **, $p \leq 0.01$, ***, $p \leq 0.001$.

(E) PD98059 did not prevent activity-dependent increases PV, GAD67, Wnt2, and Arc. PD98059 reduced but did not abolish increases in c-Fos. Values normalized to mean value at basal condition. Data are represented as mean+SEM. ANOVA followed by *t*-test. **, $p \leq 0.01$, ***, $p \leq 0.001$.

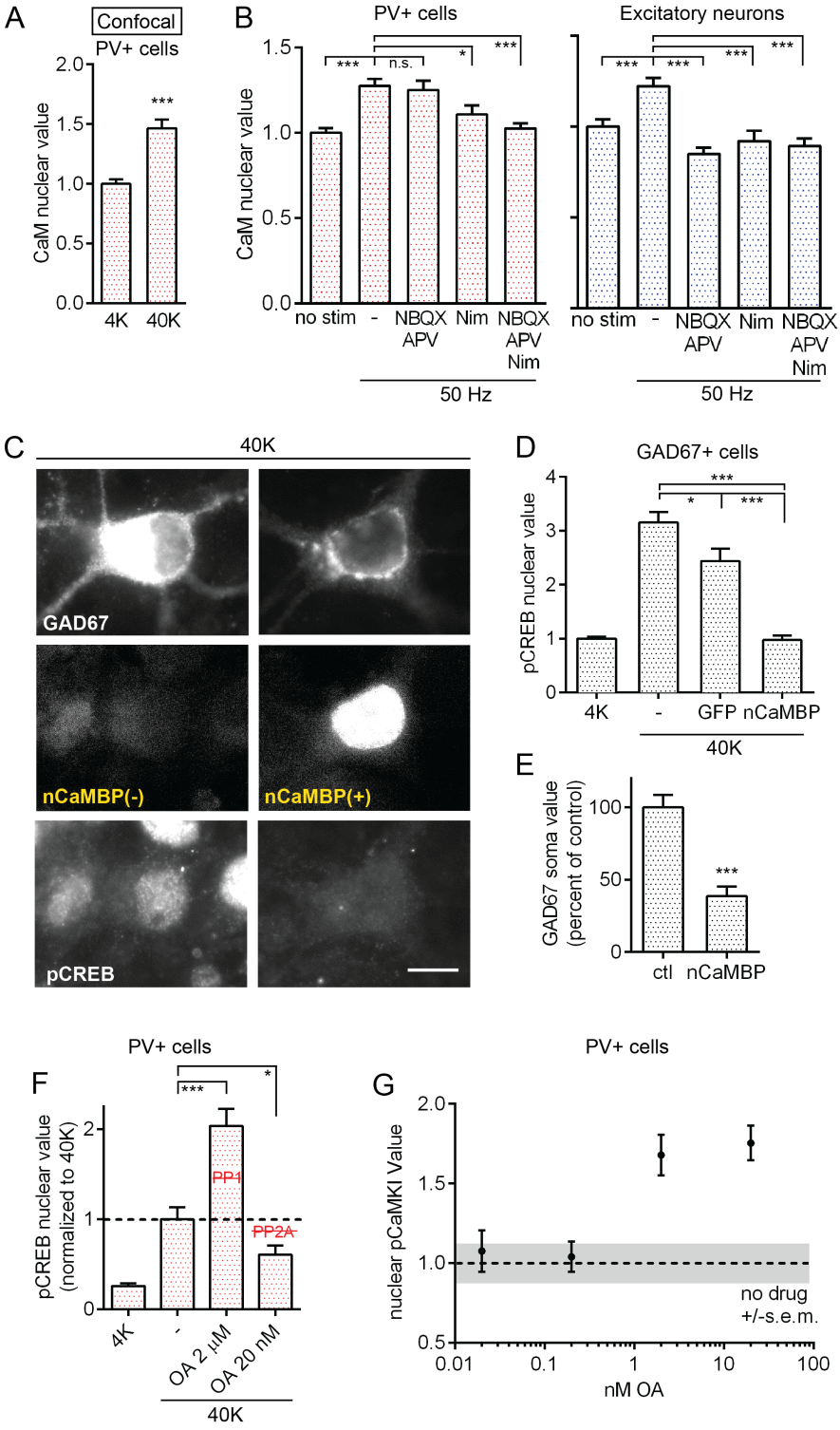

Figure S6, Related to Figure 4. CaM, PP2A, and PP1 Are Important for Nuclear Signaling in Inhibitory Interneurons

(A) Image acquisition via confocal microscopy showed that the CaM nuclear value increased in the nucleus of PV+ cells following 3 min of 40K stimulation, consistent with data from images acquired via epifluorescence microscopy (Figure 4A). Data are represented as mean+SEM. ANOVA followed by *t*-test. ***, $p \leq 0.001$.

(B) CaM nuclear value increased in PV+ cells (left panel, red) and excitatory neurons (right panel, blue) following 50 Hz stimulation for 18 s and a subsequent 42 s rest period prior to fixation. NBQX/APV blocked the increase in nuclear CaM in excitatory neurons but not PV+ cells. Nimodipine blocked the increase in nuclear CaM in both excitatory neurons and PV+ cells. All values were normalized to the mean basal condition value for each cell type. Data are represented as mean+SEM. ANOVA followed by *t*-test. *, $p \leq 0.05$, ***, $p \leq 0.001$.

(C) Representative image of a GAD67+ cell expressing nuclear CaM-Binding Protein (nCaMBP, right column) and a wild-type GAD67+ cell (left column). Note the reduced pCREB and GAD67 staining intensity in the cell expressing nCaMBP. Scale bar, 10 μm.

(D) nCaMBP expression prevented pCREB formation as compared to GFP-expressing and non-transfected control GAD67+ cells. Data are represented as mean+SEM. ANOVA followed by *t*-test. *, $p \leq 0.05$, ***, $p \leq 0.001$.

(E) nCaMBP expression resulted in reduced somatic GAD67 staining in GAD67+ cells. Data are represented as mean+SEM. ANOVA followed by *t*-test. ***, $p \leq 001$.

(F) pCREB response to 40K for 30 s was increased by okadaic acid (OA) 2 μM (blocks PP1 and PP2A), but pCREB response was attenuated by OA 20 nM (blocks PP2A only). Values normalized to 40K control. Data are represented as mean+SEM. ANOVA followed by *t*-test. *, $p \leq 0.05$, ***, $p \leq 0.001$.

(G) OA at 2 nM or 20 nM resulted in increased nuclear phospho-CaMKI (pCaMKI) at T177/178, following 1 minute of 40K depolarization. PP2A dephosphorylates CaMKI at these residues; this suggests that OA concentrations above 2 nM are sufficient to inhibit PP2A activity (and thus to obstruct CaM unloading, see text). Data are represented as mean±SEM. Grey shading represents SEM of control (non stimulated) condition.

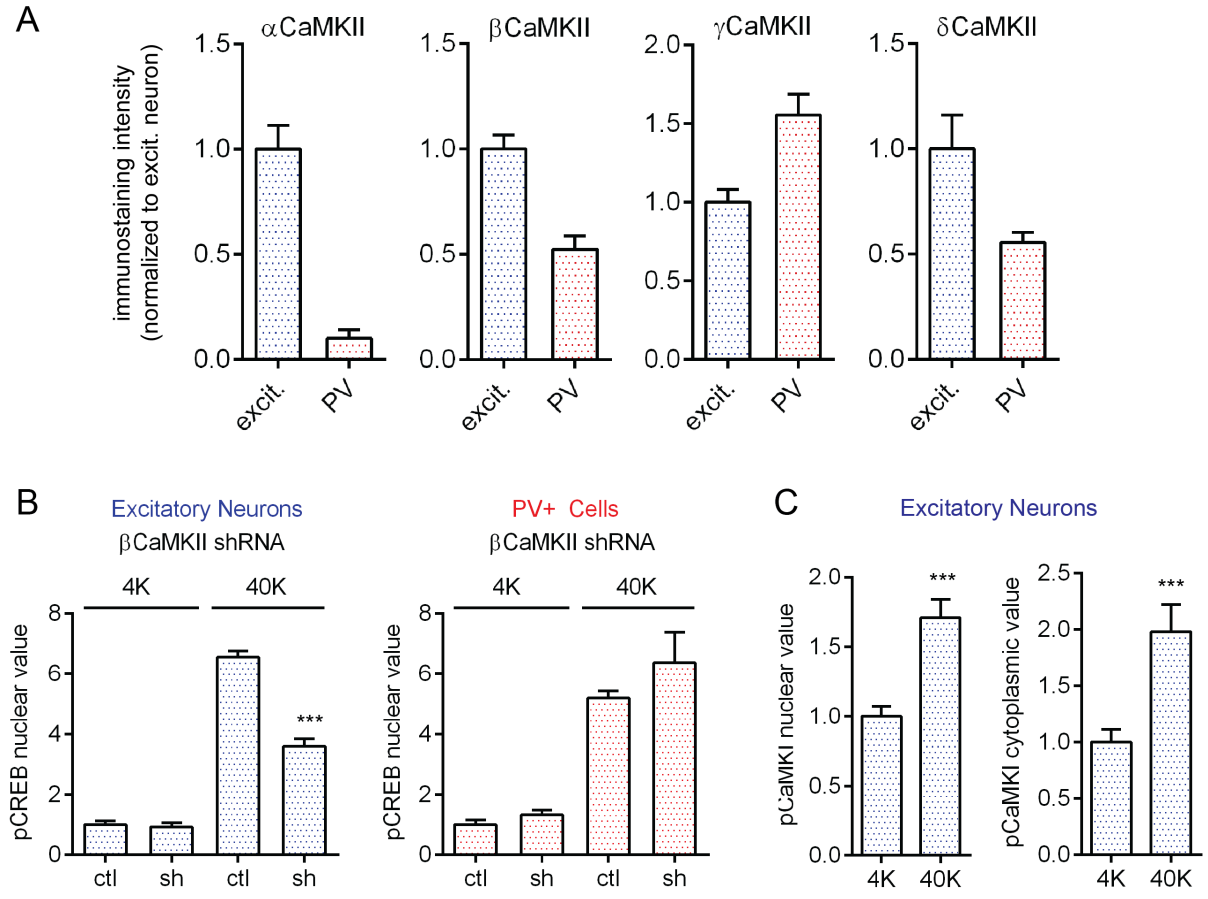

Figure S7, Related to Figures 5 and 6. Information on Roles of CaMKII and CaMKI in Cytonuclear Signaling

(A) Direct comparison of intensity of immunostaining for α-, β-, γ-, and δCaMKII between excitatory neurons (blue shading; left bar in each panel) and PV+ cells (red shading; right bar in each panel). Despite the low level of αCaMKII expression in PV+ cells (low enough to enable distinctions between inhibitory and excitatory neurons,), we were able to analyze the αCaMKII nuc/cyt ratio to verify that there was no translocation (Figure 5D). Data are represented as mean+SEM.

(B) βCaMKII shRNA knockdown reduced pCREB in response to 40K for 1 min in excitatory neurons, but not in PV+ cells. Values normalized to baseline. Data are represented as mean+SEM. ANOVA followed by *t*-test. ***, $p \leq 0.001$.

(C) phospho-CaMKI increased in both the cytoplasm and the nucleus of excitatory neurons following 3 min of 40K depolarization. Data are represented as mean+SEM. ANOVA followed by *t*-test. ***, $p \leq 0.001$.

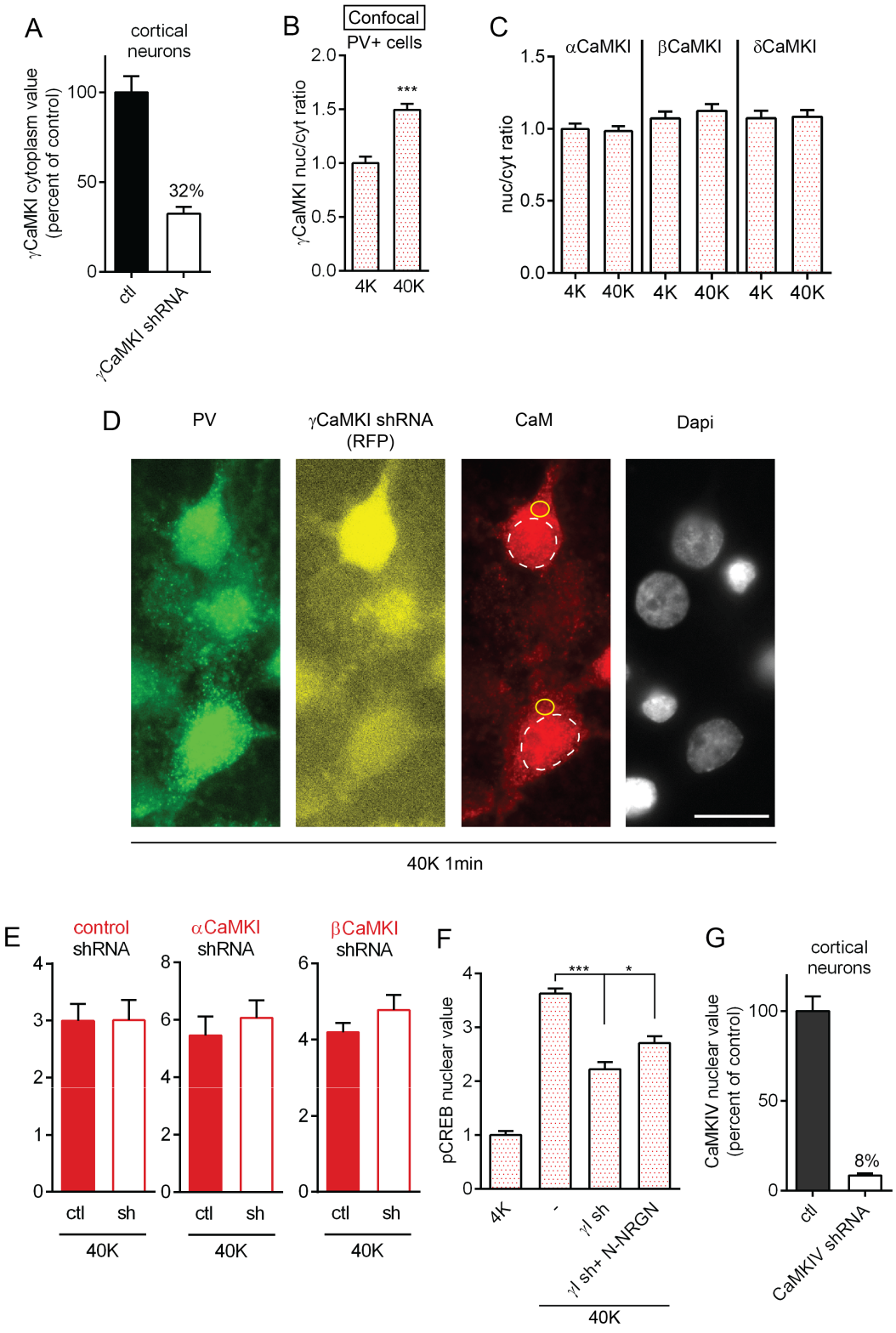

Figure S8, Related to Figures 7 and 8. Information on Roles of CaM, CaMKI, and CaMKIV in Cytonuclear Signaling in PV+ cells

(A) γCaMKI shRNA reduced cytoplasmic γCaMKI levels by ~67.6% in cortical neurons.

(B) Image acquisition via confocal microscopy showed that the γCaMKI nucleus/cytoplasm ratio increased in PV+ cells following 1 min of 40K stimulation, consistent with data from images acquired via epifluorescence microscopy. Data are represented as mean+SEM. ANOVA followed by *t*-test. ***, $p \leq 0.001$.

(C) The nuc/cyt ratio of α-, β-, or δCaMKI did not change following 2 min of 40K depolarization. Data are represented as mean+SEM.

(D) Representative image of CaM staining (red) in two PV+ neurons (green) in the same field of view, following 1 min of 40K depolarization. Only the cell at the top expresses a γCaMKI shRNA knockdown construct, as indicated by RFP signal (yellow). Dashed white line in the CaM panel represents a tracing of the Dapi counterstain (grayscale). Yellow circle is a representative ROI in the cytoplasm used for image analysis. Note the different nuclear vs cytoplasmic distributions of CaM in the shRNA-expressing cell relative to the non-transfected cell, representative of pooled data (Figure 7G). Scale bar, 20 μm.

(E) pCREB response following 40K for 30s was not affected by transfection with a control shRNA construct or with α- or βCaMKI shRNA constructs. Data are represented as mean+SEM.

(F) If γCaMKI was acting merely as a shuttle to deliver CaM to the nucleus (Ma et al., 2014), then unveiling a "caged" nuclear CaM should be sufficient to trigger pCREB. To test this, we assayed whether γCaMKI knockdown could be rescued by a nuclear-localized neurogranin (Nrgn; (Ma et al., 2014)). NLS-Nrgn binds nuclear CaM until an increase in nuclear Ca^{2+} triggers Ca^{2+}/CaM release, thus allowing 40K stimulation to trigger an increase in nuclear Ca^{2+}/CaM. NLS-Nrgn was introduced via viral injection. Co-expression of NLS-Nrgn with γCaMKI shRNA partially rescued the reduction in pCREB seen following γCaMKI knockdown. This leaves open the possibility that γCaMKI acts not only as a CaM shuttle, but also as a protein kinase in the nucleus. Data are represented as mean+SEM. ANOVA followed by *t*-test. *, $p \leq 0.05$, ***, $p \leq 0.001$.

(G) CaMKIV shRNA reduced nuclear CaMKIV levels by 91.6% in cortical neurons. Experiments with CaMKIV do not rule out the possibility that, in other contexts, CREB phosphorylation may depend on other kinases such as Rsk1+Rsk2, Msk1+Msk2, p38, PKG, AKT/PKB, or PI3K (Johannessen et al., 2004), or phosphatases such as PP1 or PP2A.

Supplemental Experimental Procedures

All procedures were approved under an NYU IACUC protocol.

In vivo *auditory stimulation.* Mice 2-3 months old (2 non-stimulated (control) mice, 2 stimulation mice; C57Bl6 background strain, PV-ires-Cre, male and female) were held >1 hour in a sound attenuation chamber. 30 minutes prior to stimulation, mice were anesthetized with an intraperitoneal injection of ketamine/xylazine (0.01 mL/g) and returned to the sound attenuation chamber. Just before stimulation, a cannulated speaker was positioned in the right ear of stimulated mice, and a 100-ms long 70 dB white noise stimulus was played at 0.5 Hz for 20 min. For control mice, no tone was played. Following stimulation, animals were injected with a lethal dose of pentobarbital (70-100 mg/kg), and perfused with cold saline followed by cold 4% paraformaldehyde. The time from the end of stimulation to paraformaldehyde perfusion was ~10 minutes. Brains were preserved in 30% sucrose, embedded in O.C.T. (optimum cutting temperature formulation of glycols and resins, Tissue-Tek®), frozen, and cut into 16 μm cryostat sections. Left primary auditory cortex (A1) was analyzed.

In vivo *electrical recording from rat cortex*. Measurement of spike rates were performed in 11 rats implanted with 64-site silicon probe electrodes (Grosmark et al., 2012). Recordings occurred over 2 to 10 hour periods while the animal was in its home environment without imposed behavioral paradigms. Behavior was primarily sleep but included interspersed ambulatory activity. Local field potential (LFP) recording was performed at 20,000 samples per second per channel and was analyzed post-hoc to extract spikes (Grosmark et al., 2012). Spikes were first automatically clustered into similar classes of events using KlustaKwik (Harris et al., 2000) and then manually reviewed thereafter to verify spike waveform quality, cluster separation and refractory periods. Finally, mean per-cluster waveforms were calculated and used to separate putative excitatory cells from putative inhibitory cells. Trough-to-peak time and spike width were measured and a 2-dimensional separatrix was created to separate putative excitatory cells with wider spikes (based on wavelet transform) and larger trough-to-peak times from the putative inhibitory neurons with narrower spikes and smaller trough-to-peak times. The separatrix was based on a dataset where optogenetically tagged PV+ cells were distinguished from other cell types (Stark et al., 2013). Spike rates of individual neurons were calculated as the number of spikes in each cluster across the entire recording period. Our analysis provides a conservative estimate of differences in spike rates between the cell types; the putative PV+ cell population may have included some regular-spiking cells, and the putative excitatory cell population may have included some PV+ cells, making the measured differences smaller than would be obtained if separation were perfect.

In vivo Ca^{2+} *imaging from mouse auditory cortex*. All procedures were approved under an NYU IACUC protocol. Mice 2-3 months old (2 mice, male and female; C57 background strain, PV-cre crossed with ai9 tdTomato reporter line) were anesthetized with isoflurane (2.0% during induction and surgery, 0.75% during auditory cortex mapping). A craniotomy was performed over the right temporal lobe and the right auditory cortex was exposed (3 mm craniotomy, centered 1.75 mm anterior to the lambda suture on the ridge line). Pure tones (70 dB SPL, 4-64 kHz, 50 ms, 3 ms cosine on/offramps, quarter-octave spacing) were delivered in pseudo-random sequence at 0.5-1 Hz. A1 location was determined by mapping multiunit responses 400-600 mm below the surface using tungsten electrodes in a sound-attenuating chamber. An adeno-associated virus (AAV) vector encoding the calcium indicator GCaMP6s (AAV1-SYN-GCAMP6s, UPENN vector core) was injected for expression in layer 2/3 neurons in right A1. Above the injection coordinates, a cranial window was implanted by replacing a circular piece of skull by a glass-coverslip (diameter=3 mm, Warner Instruments) that was secured in place using a mix of dental cement and Krazy glue. A custom-made stainless-steel headpost (Ponoko) was affixed to the skull using C&B Metabond dental cement (Parkell). Each animal was allowed to recover for at least 2-3 weeks. Two-photon fluorescence of GCaMP6s was excited at 900 nm using a mode locked Ti:Sapphire laser (MaiTai, Spectra-Physics, Mountain View, CA) and detected in the green channel (GFP emission). Imaging was performed on a multiphoton imaging system (Moveable Objective Microscope, Sutter Instruments) equipped with a water immersion objective (20X, NA=0.95, Olympus) and the emission path was shielded from external light contamination. Images were collected using ScanImage (HHMI). To image A1, the objective was tilted to an angle of 50-60˚. To record time courses of auditory-evoked neuronal activity, awake animals were head-fixed under the microscope and a speaker was placed adjacent to the microscope (microphone-ear distance ~10 cm). During auditory stimulation, ~300 μm^2 areas in layer 2/3 of A1 containing multiple GCaMP6s expressing neurons were selected and imaged (scan rate ~4 Hz, 0.26 s/frames, laser power ≤40 mW).

Juxtacellular recordings were performed in transgenic mice expressing tdTomato in PV+ neurons (PV-cre X ai9) that also received an injection of AAV1-SYN-GCAMP6s (UPENN vector core) 2-3 weeks before the imaging session. Briefly, animals were anesthetized with ketamine/xylazine and a 2 mm craniotomy was performed over right auditory cortex. Patch pipettes (3–8 MΩ) were filled with intracellular solution (135 mM K-gluconate, 5 mM NaCl, 10 mM HEPES, 5 mM MgATP, 10 mM phosphocreatine, and 0.3 mM GTP) and PV+ neurons (red fluorescent, tdTomato) that also expressed GCaMP6s (green fluorescent) were targeted using two-photon microscopy. White noise stimuli (broadband, 4-64 kHz, 70 dB) were played to the animal during recordings and images were acquired at ~4 Hz.

Primary cultures of cortical neurons. Cortical neurons were cultured from postnatal day 0 to 1 male and female Sprague-Dawley rat pups. The frontal cortex was isolated and washed twice in ice-cold modified HBSS (4.2 mM $NaHCO_3$ and 1 mM HEPES, pH 7.35, 300 mOsm) containing 20% fetal bovine serum (FBS; Hyclone, Logan, UT). Cortices were washed and digested for 30 min in a papain solution (2.5 ml HBSS + 145 U papain + 40 μl DNase) at 37°C with gentle shaking every 10 min. Digestion was stopped by adding 5 ml of modified HBSS containing 20% fetal bovine serum. After additional washing, the tissue was dissociated using Pasteur pipettes of decreasing diameter. The cell suspension was pelleted twice and filtered with a 70 μm nylon strainer, and plated on 10 mm coverslips coated with poly-D-lysine. The cultures were maintained in NbActiv4 (BrainBits, Springfield, IL). A 50% medium change was performed at 7 days, and once per week thereafter. Neurons were used 14-21 days after plating.

Ca^{2+} imaging from cultured rat cortical neurons. Cells were loaded with Fluo-4 (AM ester, Life Technologies). Two platinum electrodes were placed at a distance of ~10 mm in the 4 mM K^+ Tyrode's solution (4K) containing APV (50 μM) and NBQX (10 μM). The cultured cortical neurons on the coverslips were field-stimulated at the specified frequency and duration with square wave pulses (0.5 ms per pulse), allowing 3-4 min between bouts of stimulation. The pulse amplitude and duration were controlled by a Grass S11 stimulator. The stimulus amplitudes were set to 10 V. Images were acquired with a Zeiss LSM 510 meta Imager.M1 confocal microscope at 1.67 Hz. Ca^{2+} imaging experiments were analyzed using Icy software.

*Drug treatments and stimulation***.** To induce CREB phosphorylation, we stimulated cortical neurons with the indicated high [K^+] solution at 37°C for 1 to 300 s, then fixed the cells (in 4% paraformaldehyde in PBS, with 20 mM EGTA and 4% (w/v) sucrose), either immediately after the stimulation), or after the cells had been incubated in culture media for 90 min at 37°C. Where indicated, drugs were added 30 min before and included throughout the stimulation. All K^+-rich stimulation solutions contained 0.5 μM TTX (Ascent Scientific) to block action potentials, as well as 10 μM NBQX (Ascent Scientific) and 50 μM APV (Ascent Scientific) to block AMPA and NMDA receptors, respectively. 4K Tyrode's consisted of (in mM): 150 NaCl, 4 KCl, 2 $MgCl_2$, 2 $CaCl_2$, 10 HEPES, 10 glucose, pH 7.4. When stimulating with elevated [K^+], Na^+ was adjusted to maintain osmolarity. To block calcineurin, Cyclosporine A (Tocris) was used at 50 nM; to block CaM Kinases, KN93 (Tocris) was used at 4 μM; KN92 (Tocris) was used at 4 μM; to block Ca_V1 channels, nimodipine (Abcam) was used at 10 μM; to block CaMKK, STO609 (Tocris) was used at 3.3 μM; to block MEK1, PD98059 (Tocris) was used at 50 μM; to block PP2A, okadaic acid (Tocris) was used at 20 nM; to block PP1 and PP2A, okadaic acid (Tocris) was used at 2 μM; to block PKA, KT5720 (Tocris) was used at 200 nM; to block PKC, bisindolylmaleimide I GF 109203X (Cayman) was used at 10 μM; to block P2 receptors, PPADS (Tocris) was used at 30 μM. Cells were loaded with Ca^{2+} chelators EGTA-AM and BAPTA-AM (Life Technologies), used at 200 μM along with 1:1000 Pluronic F-127 (Life Technologies), 45 min before stimulation.

For pCREB staining following field stimulation, the same protocol was followed as with the Ca^{2+} imaging, except cells were pre-treated with TTX for 30 min prior to stimulation but removed from TTX during stimulation. Cells were fixed immediately following the end of the stimulus unless otherwise indicated.

DNA constructs. Constructs for knockdown of CaMKIV, αCaMKI, γCaMKI, overexpression of CaMKIV and γCaMKI, and the negative shRNA control were gifts from Sayaka Takemoto-Kimura and Haruhiko Bito (Ageta-Ishihara et al., 2009; Takemoto-Kimura et al., 2007). Constructs for the knockdown of βCaMKI were a gift from Gary Wayman. Arc shRNA was purchased from OriGene. CA-CaMKIV construct is a truncated mouse CaMKIV313 (NM_009793.3) with a FLAG tag on the C terminus. DN-CaMKIV is a K75E mutation of human CaMKIV (NM_001744.4) with a FLAG tag on the N terminus. CaMBP4 (nCaMBP) has four MKRRWKKNFIAVSAANRFKK sequences with a C-terminal FLAG tag. A description of the generation of the γCaMKII knockdown construct and the HA-tagged-NLS-Nrgn (NLS-Nrgn) can be found in (Ma et al., 2014).

Transfection. Cortical neurons were transfected 6 days after plating using a high efficiency Ca^{2+}-phosphate transfection method (Jiang and Chen, 2006).

Immunocytochemistry and immunohistochemistry. 16 μm cryostat sections were blocked in 10% normal donkey serum with 0.2% Triton X-100, and incubated in 1% normal donkey serum with 0.1% Triton X-100 and primary antibodies for 40 hours at 4°C. Slices were washed in PBS (3x15 min), and incubated in 1% normal donkey serum with 0.1% Triton X-100 and secondary antibodies for 2 hours. Slices were washed in PBS (3x15 min), mounted as above, and imaged on a confocal microscope as above.

Fixed cultured neurons were then permeabilized with 0.1% Triton X-100, blocked with 6% normal donkey serum and incubated overnight at 4°C in primary antibodies: rabbit anti-Arc (1:1000, 156 003, Synaptic Systems); mouse anti-CaM (1:10000, 05-173, Millipore); mouse anti-CaMKI (1:50, sc-377418, Santa Cruz); rabbit anti-pCaMKI (1:500, sc-28438-R, Santa Cruz); rabbit anti-δCaMKI (1:500, sc-134638, Santa Cruz); mouse anti-γCaMKI (1:1000, 77046, Abcam); rabbit anti-γCaMKI (1:200; PA5-19661, Thermo Scientific); mouse anti-αCaMKII (1:1000, 13-7300, Invitrogen); rabbit anti-αCaMKII (1:1000, 50202, Abcam); mouse anti-βCaMKII (1:1000, 13-9800, Invitrogen); goat anti-γCaMKII (1:500, sc-1541, Santa Cruz); goat anti-δCaMKII (1:500, sc-5392, Santa Cruz); rabbit anti-pCaMKIV (1:500, sc-28443-R, Santa Cruz); mouse anti-CaMKIV (1:500, sc-136249, Santa Cruz); rabbit anti-αCaMKK (1:333, sc-11370, Santa Cruz); rabbit anti-βCaMKK (1:250, sc-50341, Santa Cruz); rabbit anti-c-fos (1:1000, 2250, Cell Signaling); mouse anti-GAD67 (1:1000, MAB5406, Millipore); rabbit anti-parvalbumin (1:5000, PV-27, Swant); goat anti-parvalbumin (1:5000, PVG-214, Swant); mouse anti-pCREB (1:333, 9191, Cell Signaling); rabbit anti-pCREB (1:333, 9198, Cell Signaling); goat anti-pCREB (1:333, sc-7978, Santa Cruz). The next day, cells were washed with PBS (3x5 min), incubated at room temperature for 50 min with Alexa secondary antibodies (1:1000, Molecular Probes), washed with PBS (3x5 min) and mounted using ProLong Gold (with or without Dapi)(Invitrogen). The cells were imaged with a 63X (1.3 NA) oil objective on an Axioplan epifluorescence microscope equipped with an AxioCam digital camera using AxioVision or on a Zeiss LSM 510 meta Imager.M1 confocal microscope.

Image Analysis. In quantum dot experiments to assess the thickness of optical sectioning with our epifluorescence microscope (Zeiss Imager M.2), QDs emitting light at 655 nm were plated at low density on a glass coverslip. The long wavelength provides a conservative estimate of the width of the point spread function, in contrast to shorter wavelengths of emitted light such as 520 nm. Among all fluorophores used in this study, fluorescence at 647 nm has the greatest s parameter of the point spread function (Zhang et al., 2007). A z-stack was collected with our epifluorescence microscope, with image acquisition every 50 nm and the average intensity of QD luminescence was calculated as a function of $|\Delta z|$-location (Figure S3D).

For pCREB staining in slices, maximum intensity projections of z-stacks were analyzed and cells were counted using ImageJ (NIH). Images for immunostaining experiments in culture were analyzed using a custom-written macro in ImageJ (NIH) to analyze the pixel intensity of immunostaining. The nuclear marker DAPI and an antibody against a molecular marker for a specific cell type were used to delineate the nucleus and cell body, respectively. For most analysis, a region of interest (ROI) adjacent to each neuron, but not in the neuron, was selected and used as an 'off-cell' background. The nuclear staining intensity in each neuron was calculated by subtracting the average channel intensity in the 'off-cell' background ROI from the average intensity in the nuclear ROI for each neuron. The nuclear:cytoplasmic ratio was calculated as follows: [nuclear immunoreactivity- background immunoreactivity] / [somatic non-nuclear immunoreactivity- background immunoreactivity]. Data from each trial were normalized, so that different trials could be combined. Data were either normalized to the baseline value, or occasionally to the maximum value. This normalization process does not affect the meaning of the data.

For Arc staining in Figure 3D and S5C, the average pixel intensity of ROI in the dendrite (the same distance away from the cell body for all cells, <40 μm away) was recorded. A background ROI was chosen and the average pixel intensity was subtracted from the dendrite value. Arc staining was always visible, even in the basal condition, prior to stimulation.

Sholl analysis was performed using the Sholl Analysis plugin to ImageJ, followed by neuron tracing using the NeuronJ plugin.

Statistical Analysis. Statistical analyses were performed using Prism 6.0 (GraphPad software). Student's *t*-test was used for comparisons between two groups. One- or two-way analysis of variance (ANOVA) was used for analysis between three or more groups (notably, between replicates of each experiment) and a *t*-test was only used after an ANOVA showed significance. Pearson Correlation was used for correlation analysis. The Kolmogorov-Smirnov (K-

S) test was used for analysis of the distribution of CaMKIV levels. All data are shown as mean ± standard error of the mean (SEM), unless otherwise mentioned. ≥ 24 neurons were scored from 2-3 separate experiments, unless otherwise noted.

Phosphorylation Site Prediction performed using Group-based Prediction System (GPS) software (Xue et al., 2005).

Supplemental References

Ageta-Ishihara, N., Takemoto-Kimura, S., Nonaka, M., Adachi-Morishima, A., Suzuki, K., Kamijo, S., Fujii, H., Mano, T., Blaeser, F., Chatila, T.A., *et al.* (2009). Control of cortical axon elongation by a GABA-driven Ca2+/calmodulin-dependent protein kinase cascade. The Journal of neuroscience : the official journal of the Society for Neuroscience 29, 13720-13729.

Grosmark, A.D., Mizuseki, K., Pastalkova, E., Diba, K., and Buzsaki, G. (2012). REM sleep reorganizes hippocampal excitability. Neuron 75, 1001-1007.

Harris, K.D., Henze, D.A., Csicsvari, J., Hirase, H., and Buzsaki, G. (2000). Accuracy of tetrode spike separation as determined by simultaneous intracellular and extracellular measurements. J Neurophysiol 84, 401-414.

Xue, Y., Zhou, F., Zhu, M., Ahmed, K., Chen, G., and Yao, X. (2005). GPS: a comprehensive www server for phosphorylation sites prediction. Nucleic Acids Res 33, W184-187.

Zhang, B., Zerubia, J., and Olivo-Marin, J.C. (2007). Gaussian approximations of fluorescence microscope point-spread function models. Appl Opt 46, 1819-1829.